RSC Advances

ROYAL SOCIETY OF CHEMISTRY

www.rsc.org/advances

Effect of surface species and structure on the performance of CeO_2 and SO_4^{2-} doped MCM-41 catalyst toward NH_3-SCR

Zhongxian Song [a], Xiang Wu [b], Qiulin Zhang [a*], Ping Ning [a**], Jie Fan [a], Xin Liu [a], Qixian Liu [a], Zhenzhen Huang [c]

([a]*Faculty of Environmental Science and Engineering, Kunming University of Science and Technology. Kunming, 650500, P.R. China*; [b]*Yunnan TianAn Chemical Co., Ltd., Anning, 650309, P.R. China*; [c]*College of Environmental Science and Engineering, Hunan University, Changsha 410082, P.R. China*)

* Corresponding author. Tel:+ 86-871-65170905.

E-mail address:qiulinzhang_kmust@163.com; ningping_58@126.com

Abstract: The present work elucidated the effect of structures and surface species on the activity of CeO_2 and SO_4^{2-} doped MCM-41 catalysts toward NO reduction by NH_3. The results indicated that the sulfated species were generated over Cat-A ($Ce(NO_3)_3 \cdot 6H_2O$ and H_2SO_4 simultaneously doped on MCM-41) and Cat-B ($Ce(NO_3)_3 \cdot 6H_2O$ firstly immerged to MCM-41 and followed by impregnation of H_2SO_4) except for Cat-C (H_2SO_4 firstly doped onto MCM-41 and followed by $Ce(NO_3)_3 \cdot 6H_2O$). The sulfation contributed to the formation of Ce^{3+} concentration, oxygen vacancies and surface acidity, resulting in the improvement of SCR activity. However, the positive influence on the SCR activity was overwhelmed by the decomposition of sulfated species. The apparent activation energy of Cat-A (60 kJ/mol) was much lower compared with that of Cat-B and Cat-C (71 and 78 kJ/mol, respectively). The pore structures and surface species were responsible for the SCR activity over the CeO_2 and SO_4^{2-} doped MCM-41 catalysts. The best catalytic activity was obtained over Cat-A, followed by Cat-B, and Cat-C exhibited the least catalytic activity.

Keywords: structure and surface species; MCM-41; apparent activation energy; sulfated species

1. Introduction

Nitrogen oxide species (NO_x) emission from flue gases of stationary sources are one of important pollutants in the air, which not only cause various environmental problems such as greenhouse effects, acid rain and photochemical smog, but also affect the human health [1]. With the stringent NO_x emission legislation, many strategies have been implemented for controlling NO_x emission. Among the NO_x removal technologies, the selective catalytic reduction (SCR) of NO_x by NH_3 is one of the most widely used technologies for the controlling of NO_x from stationary resources, and the commercial catalyst is V_2O_5-WO_3 (MoO_3)/TiO_2 [2, 3]. However, the potential volatility and intense toxicity of vanadium oxide are harmful to the human health and environment [4, 5]. Consequently, great efforts have been made to develop environmentally-friendly SCR catalysts.

In recent years, the mesoporous materials have been extensively used for catalyst support due to their large specific surface area, favored pore diameter and ordered framework [6]. MCM-41, a typical representative in mesoporous materials, possesses potential catalytic applications. It is well known that pure MCM-41 mesoporous molecular sieves is restrained in industry application due to some disadvantages, such

as inefficient catalytic activity and weak surface acidity. However, pure MCM-41 can be modified by some transition metals, remarkably improving the catalytic activity and the surface acidity [7-11]. Liu et al. [11] have reported that the Cu/MCM-41 catalysts exhibited excellent catalytic activity in the NO-SCR reaction. Wan et al. [12] also have revealed that the high catalytic activity of Cu-Al-MCM-41 modified by Cu and Al species was obtained in C_3H_6-SCR reaction. Besides, Qiu et al. [13] investigated the effect of Cu contents on the NH_3-SCR activity over MCM-41 catalysts. Ziolek et al. [14] reported that the surface acidity could be improved by the introduction of Nb into MCM-41 in the NH_3-SCR reaction. Meanwhile, few works have been done to study the effect of structures and surface species on the SCR activity over MCM-41 modified by some transition metals in NH_3-SCR reaction.

Recently, CeO_2-based catalysts have been extensively investigated due to excellent oxygen storage capacity and redox ability in NH_3-SCR reaction. Furthermore, the supported SCR catalysts are dramatically influenced by the kinds of surface species and the structures of supports. Excellent dispersion of active CeO_2 particles, which contributes to the redox ability and surface acidity, can be facilitated by the favored structure of MCM-41, resulting in improvement of the catalytic activity in the NH_3-SCR reaction. Therefore, the structures and surface species of MCM-41 modified by CeO_2 should be intensively studied.

Sulfate modification is an effective method to increase the catalytic activity for the improvement of surface acidity over CeO_2-based catalysts [15-18]. But the effect of sulfated CeO_2 on the structures and SCR performances over MCM-41 is few investigated. It is widely accepted that the surface species and structures of the support catalysts are remarkably affected by the metal-loading procedure, resulting in the different catalytic activities [19, 20]. Thereby, the effect of CeO_2 and SO_4^{2-} doped MCM-41 on the SCR activity is investigated in the NH_3-SCR reaction.

In this work, the CeO_2 and SO_4^{2-} doped MCM-41 supports were prepared by impregnation method. The specific surface area, pore structures, surface species and the catalytic activity were investigated. Furthermore, the characteristics of samples were explored by XRD, NH_3-TPD, TGA, N_2 adsorption-desorption, H_2-TPR, Raman and XPS.

2. Experimental

2.1 Catalyst preparation

MCM-41 supports were purchased from Nanjing Xian-feng nanomaterials

technology Co., Ltd. $Ce(NO_3)_3 \cdot 6H_2O$ and H_2SO_4 were purchased from Sinopharm Chemical Reagent Co., Ltd, both of them were analytical grade. The CeO_2 and SO_4^{2-} doped MCM-41 were prepared by wet impregnation method. Firstly, the $Ce(NO_3)_3 \cdot 6H_2O$ (1.5 g) and 0.1 g/mL H_2SO_4 (3 mL) were simultaneously dissolved in deionized water (3 mL). And then 2.1 g of the MCM-41 supports were immersed. The mixture was kept at 60 °C for 5 h and dried for 12 h at 105 °C. The powders were calcined at 550 °C for 5 h in air. The catalysts were named as Cat-A. Secondly, the 0.1 g/mL H_2SO_4 (3 mL) was dissolved in deionized water (3 mL). And then 2.1 g of the MCM-41 supports were added. The above powder was maintained at 60 °C for 5 h, dried for 12 h at 105 °C and calcined at 550 °C for 5 h in air. The obtained powders were put into the 1.5 g $Ce(NO_3)_3 \cdot 6H_2O$ again. The above powders were immersed at 60 °C for 5 h, dried for 12 h at 105 °C and calcined at 550 °C for 5 h. The catalysts were signed as Cat-B. Thirdly, the process was the same as Cat-B, but the impregnation sequence of $Ce(NO_3)_3 \cdot 6H_2O$ and H_2SO_4 was opposite. The 1.5 g $Ce(NO_3)_3 \cdot 6H_2O$ was first immersed, and followed by 0.1 g/mL H_2SO_4 (3 mL) solution. The catalyst was marked as Cat-C.

2.2 Catalyst characterization

The powder X-ray diffraction (XRD) measurements were operated on a Rigaku D/Max 2500 system between 10º and 70º at a step of 6º min^{-1} by using Cu Kα (40 kV, 100 mA) radiation to determine the crystal structure.

Raman spectra (RS) were performed on a Renishaw-2000 Raman spectrometer at a resolution of 2 cm^{-1} by using the 514.5-nm line of an Ar ion laser as the excitation source.

TGA experiments were carried out on Simultaneous Thermal Analyzer (DTG-60H) with 0.009 mg samples under a nitrogen flow of 10 mL/min. The temperature increased from 50 to 900 °C at a rate of 10 °C/min.

The specific surface areas of the catalysts were obtained at -196 °C using a Tristar□3020 automated gas sorption system. Prior to N_2 measurement, the catalysts were degassed at 300 °C for 4 h. The specific surface areas were measured by Brunauer-Emmett-Teller (BET) model. Average pore diameters and total pore volumes were obtained from the desorption branches of the isotherms by Barrett-Joyner-Halenda (BJH) method.

X-ray photoelectron spectroscopy (XPS) was performed in an ULVAC PHI 5000 Versa Probe-□equipment operating at 10^{-9} Pa with an Al Kα radiation (1486.6

eV) to analyze the chemical states and the surface atomic concentration of the catalysts. The observed spectra were corrected with the C 1s binding energy value of 284.8 eV.

The H_2 temperature-programmed reduction (H_2-TPR) experiment was operated on a GC-9750 equipped with a thermal conductivity detector. Before the H_2-TPR experiment, the catalysts were pretreated in pure N_2 at 400 ℃ for 60 min and cooled to 100 ℃. The H_2-TPR runs were operated in a flow of 5 vol.% H_2/Ar (30 ml min^{-1}) from 100 to 900 ℃ with a heating rate of 10 ℃/min.

The temperature programmed desorption of ammonia (NH_3-TPD) of samples was carried out in order to investigate the surface acidity on gas chromatography with a thermal conductivity detector (TCD) setup (Fuli, GC-9750, China). Before the test, the samples were pretreated in N_2 at 400 ºC for 45 min, followed by introduction of 5% NH_3/N_2 at a flow rate of 30 mL/min for about 60 min. Desorption was performed by heating from100 to 450 ºC with a heating rate of 10 ºC/min.

2.3 Activity test

The SCR activity measurements were operated in a fixed-bed quartz reactor (8 mm i.d.) with 0.4 mL catalysts. The experiments were performed at 150-450 ℃ and the gas flow was measured by mass flow meters. The reactant gas composition was as follows: 600 ppm NO, 600 ppm NH_3, 5 vol.% H_2O (when used), 50 ppm SO_2 (when used), 5 vol% O_2 and N_2 balance. The total flow rate was 400 mL/min, corresponding to a gas hourly space velocity of 60 000 h^{-1}. The concentrations of NO_x and NH_3 were continuously measured by the ECOM·J2KN and GXH-1050E flue gas analyzer, respectively. The N_2O species were analyzed by gas chromatograph (Fuli, 9790). To minimize the effect of gas adsorption on the catalysts, the reaction system was kept for 30 min at each reaction temperature to reach a steady state before analysis.

3. Results and Discussions

3.1 XRD analysis

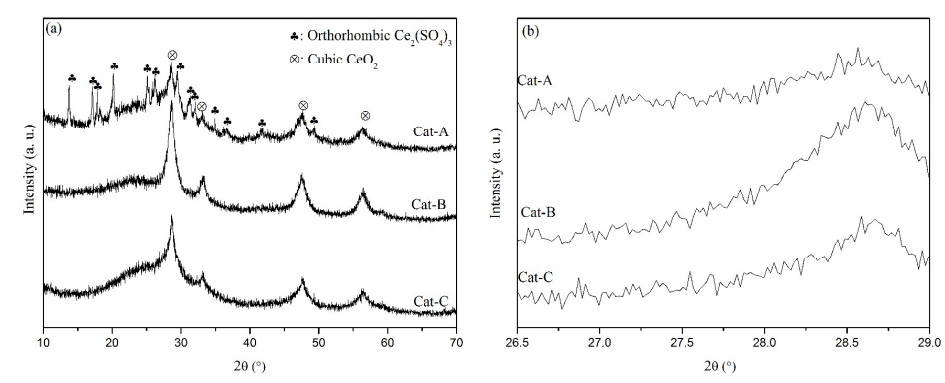

Fig. 1 XRD patterns of different catalysts.

The XRD patterns of Cat-A, Cat-B and Cat-C catalysts were shown in Fig. 1a. The XRD pattern of Cat-A exhibited the presence of cubic CeO_2 phase (PDF: 43-1003), together with orthorhombic $Ce_2(SO_4)_3$ (PDF: 52-1494) peaks. The Cat-B and Cat-C catalysts merely showed XRD peaks corresponded to cubic CeO_2 phase (PDF: 43-1003). No sulfated species were observed over Cat-B and Cat-C catalysts, which indicated the sulfated species were in the forms of highly dispersed state or clustered state, which were too small to be detected by XRD instrument over the two samples. Besides, the strength peaks of Cat-B and Cat-C were higher than that of Cat-A, and the value of FWHM (full width at half maximum) over Cat-A in Table 1 was larger than that of Cat-B and Cat-C, suggesting that Cat-B and Cat-C possessed higher crystallinity than Cat-A. According to Zhang et al. reports [21], the lattice parameter could be served as a function of the particle sizes of catalysts, and the lattice parameter would increase with a decrease in particle sizes of catalysts. Therefore, the lattice parameter *a* was calculated in the 2θ range of 27-30° in Fig. 1b for the catalysts, and the results were presented in Table 1. It was obvious that the lattice parameter *a* of Cat-A was larger than that of Cat-B and Cat-C. The phenomenon reflected that the Cat-A catalyst possessed smaller particle sizes in comparison with Cat-B and Cat-C.

Table 1 Lattice parameter and FWHM of Cat-A, Cat-B and Cat-C catalysts.

Sample	FWHM	2θ/º	Lattice parameter *a*/Å
Cat-A	1.35	28.55	5.408
Cat-B	1.20	28.67	5.386
Cat-C	1.28	28.64	5.393

3.2 N_2 adsorption-desorption isotherms

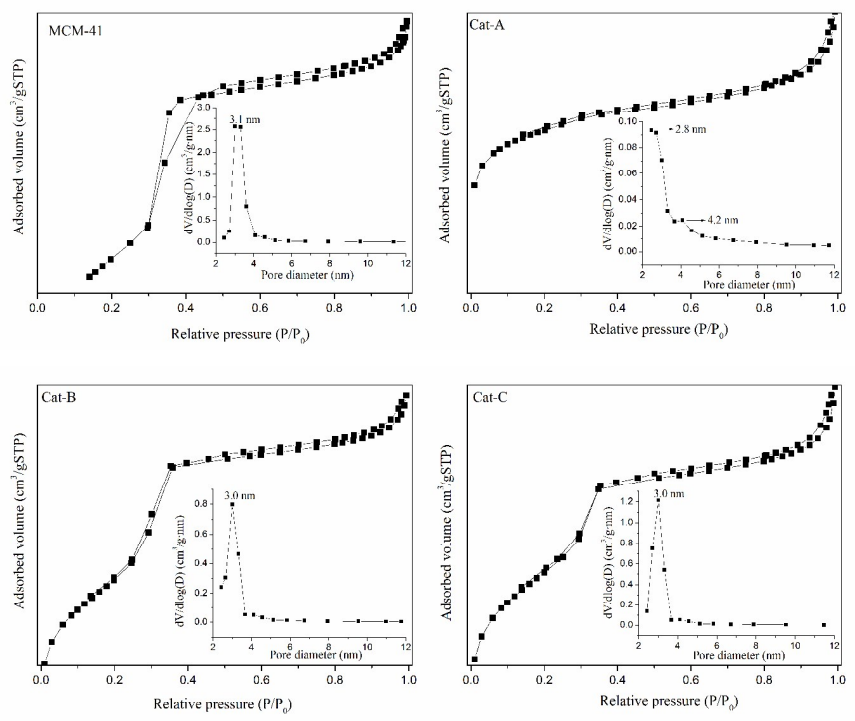

Fig. 2 N_2 adsorption-desorption results of the catalysts

Fig. 2 showed the nitrogen adsorption-desorption isotherms and the BJH pore size distribution curves of the catalysts. It was clear from the Fig. 2 that all the catalysts showed type IV isotherms (according to IUPAC classification), which was the typically characteristic of mesopores (2-50 nm) [22]. For the Cat-B and Cat-C samples, there were two regions of hysteresis: one at P/P_0 >0.35 and the other one at 0.2, which suggested that more abundance of micropores and mescopors existed over these two samples. Furthermore, the appearance of a H2 hysteresis loop was observed over pure MCM-41 with ink-bottle-type pores where large cavities were connected by narrow channels [23, 24]. However, the hysteresis loop was absent over Cat-A, Cat-B and Cat-C catalysts. In other words, the adsorption isotherm was nearly coinciding with the desorption isotherm over the three samples. The phenomenon indicated that the pores of Cat-A, Cat-B and Cat-C were open pores [25, 26]. After the simultaneously introduction of $Ce(NO_3)_3 \cdot 6H_2O$ and H_2SO_4, profile of the curve over Cat-A changed. The volume of adsorbed N_2 also decreased, indicating the remarkable reduction of total pore volume and specific surface area, as shown in Table 2. In brief, the pore

structures of Cat-A, Cat-B and Cat-C have changed due to the introduction of $Ce(NO_3)_3 \cdot 6H_2O$ and H_2SO_4 inside the framework of MCM-41. Fig. 2 also showed the BJH pore size distributions of the samples. The Cat-A catalyst mainly showed mesopores and exhibited distribution peaks near 2.8 and 4.2 nm, and the desorption pore size distributions of Cat-B and Cat-C were 3.0 nm. Besides, a dramatical decrease in the N_2 desorption differential pore volumes per weight ($cm^3/g \cdot nm$) of Cat-A was observed when compared with Cat-B and Cat-C. This meant that the abundant mesopores disappeared over the Cat-A catalyst, resulting in a decrease in BET surface area.

Table 2 BET measurements for the catalysts.

Samples	BET (m^2/g)	Total pore volume (cm^3/g)	Average pore diameter (nm)
MCM-41	952	1.0452	3.47
Cat-A	336	0.1302	6.75
Cat-B	555	0.4598	3.34
Cat-C	519	0.3665	3.84

Table 2 showed the structure properties such as the BET surface area, the average pore diameter and the BJH desorption pore volume of the samples from the N_2 physisorption results. The BET surface areas of the MCM-41, Cat-A, Cat-B and Cat-C were 952, 336, 555 and 519 m^2/g, respectively. After addition of CeO_2 and SO_4^{2-}, the BET surface area of pure MCM-41 decreased remarkably. The total pore volume decreased according to the sequence: Cat-A (0.1302 cm^3/g) < Cat-C (0.3665 cm^3/g) < Cat-B (0.4598 cm^3/g) < MCM-41 (1.0452 cm^3/g). The average pore diameter was shown as follows: 6.67 nm for Cat-A > 3.84 nm for Cat-C > 3.34 nm for Cat-B. It was obvious that the BET surface areas and total pore volume of Cat-A, Cat-B and Cat-C both remarkably decreased compared with those of pure MCM-41, which indicated that the mesopores of the MCM-41 support were blocked by the aggregated $Ce_2(SO_4)_3$, the separated CeO_2 and SO_4^{2-} species, leading to the disappearance of small pore and then a dramatically decrease in BET surface area. Based on the above discussion, the catalysts with the same composition but different impregnation sequences showed the significantly different pore structure. It was reasonably speculated that the structure properties of Cat-A, Cat-B and Cat-C

catalysts were noteworthy affected by the surface species over the samples.

3.3 Raman

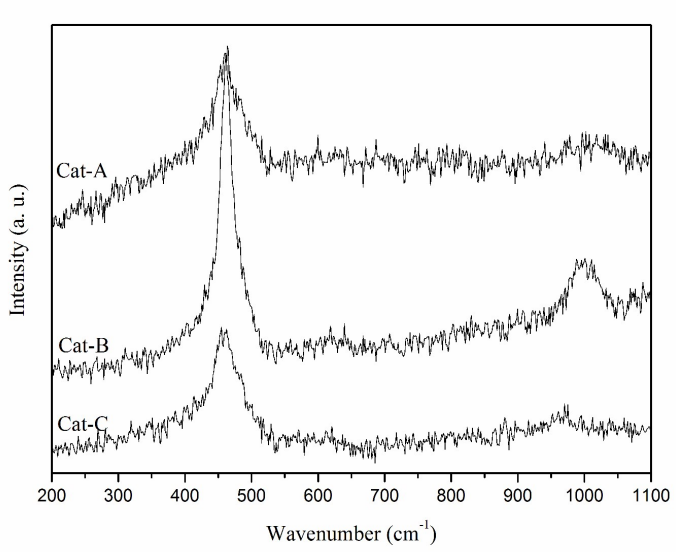

Fig. 3 Raman profiles of the catalysts.

The Raman spectra were shown in Fig. 3. It was obvious that all of samples were dominated by the main band at 460 cm^{-1}, which was attributed to the F2g mode of fluorite-type CeO_2 [27]. The bands at 1005 cm^{-1} corresponded to the reflection of sulfate group over Cat-A and Cat-B catalysts [16]. However, the sulfate species were not observed over Cat-C. In comparison with the Cat-B and Cat-C catalysts, the Cat-A catalyst not only showed a decrease in the intensity of the band at 460 cm^{-1}, but also an increase in the FWHM value. Ilieva et al. [28] reported that an increase in the FWHM value was ascribed to defect formation or the small crystal size in the CeO_2 structure. In addition, these observables in width of the F2g mode implied the effect of oxygen vacancies and inhomogeneous strain (related to the existence of low-valent cerium states). Wang et al. [29, 30] also proved that the shift and width in the main F2g mode band was closely related to the presence of reduced states of cerium. These indicated that the surface species and structures depended on the impregnation sequence of CeO_2 and SO_4^{2-} species over MCM-41.

3.4 TGA analysis

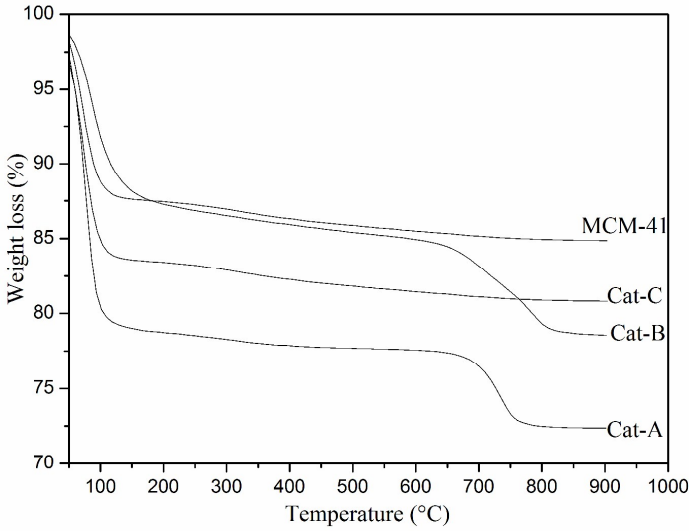

Fig. 4 Thermo-gravimetric analysis of the catalysts.

In order to investigate the effect of structures and surface species on the SCR activity over the Cat-A, Cat-B and Cat-C catalysts, thermo-gravimetric analysis (TGA) was applied and the results were shown in Fig. 4. It was obvious that the whole temperature range could be divided into two stages:

In the first stage at 30-250 °C, the remarkable weight loss was observed over the three samples, corresponding to the desorption of physical adsorbed water and dehydroxylation [16]. And the weight loss was shown as follows: MCM-41 (12.5%) < Cat-B (13%) < Cat-C (17%) < Cat-A (21.6%).

The second stage was about at 600-900 °C. For the Cat-A and Cat-B catalysts, a weight loss was observed, respectively. This weight loss was attributed to the decomposition of $Ce_2(SO_4)_3$ [31]. However, no weight loss was found over the Cat-C catalyst, implying that there was no formation of $Ce_2(SO_4)_3$.

3.5 XPS analysis

Table 3 Surface atomic concentration of the catalysts from the XPS results (atomic %).

Samples	Surface atomic concentration (atomic %)					
	Ce	S	Si	O	$Ce^{3+}/(Ce^{4+} + Ce^{3+})$	$O_\alpha/(O_\alpha + O_\beta)$
Cat-A	2.8	0	20.85	76.35	24	67.7
Cat-B	1.13	0	25.07	73.80	17.8	73.7

Cat-C	4.87	0	19.67	75.46	16.3	59.4

The atomic concentrations of the catalysts were presented in Table 3. According to the XPS results, it was obvious that the surface atomic concentration of Ce over Cat-C was the highest, followed by Cat-A and Cat-B showed the lowest surface atomic concentration. Interestingly, the surface S atomic concentration (provided in SI) was not detected over the three catalysts, which indicated that the sulfated species were likely to insert into the MCM-41 pore.

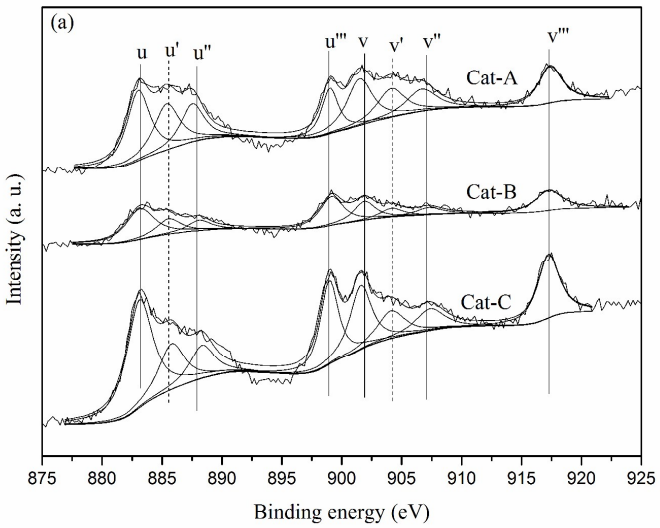

Fig. 5a Ce 3d XPS spectra of the catalysts.

The Ce 3d XPS spectra of the Cat-A, Cat-B and Cat-C samples were shown in Fig. 5a. The u, u″, u‴, v, v″, v‴ peaks were attributed to Ce^{4+} state while the u′ and v′ peaks corresponded to Ce^{3+} state [32, 33]. It was well known that the CeO_2-based catalysts showed the outstanding reducibility via the redox shift between Ce^{4+} and Ce^{3+}, and then improved the oxygen storage/release capacity. Thereby, the surface Ce^{3+} and Ce^{4+} concentrations were calculated and the results were shown in Table 3. The $Ce^{3+}/(Ce^{3+} + Ce^{4+})$ ratio ranked in the sequence of Cat-A (24%) > Cat-B (17.8%) > Cat-C (16.3%). Besides, the Ce^{3+} enrichment over Cat-A was ascribed to the appearance of lattice defects or oxygen vacancies. Combined with XRD results, the $Ce_2(SO_4)_3$ species were observed. But the S species were not detected over the Cat-A catalyst from Table 3. These further confirmed that the sulfation could not exist at the outer surface of MCM-41 modified by $Ce(NO_3)_3 \cdot 6H_2O$ and SO_4^{2-} species. The sulfation could not only serve as a stabilizer of oxygen vacancies during the impregnation and calcination process, but also contributed to reducing the oxidation

state of the surface cations [34, 35]. Thus, the surface Ce^{3+} concentration of Cat-A was improved when compared with those of Cat-B and Cat-C.

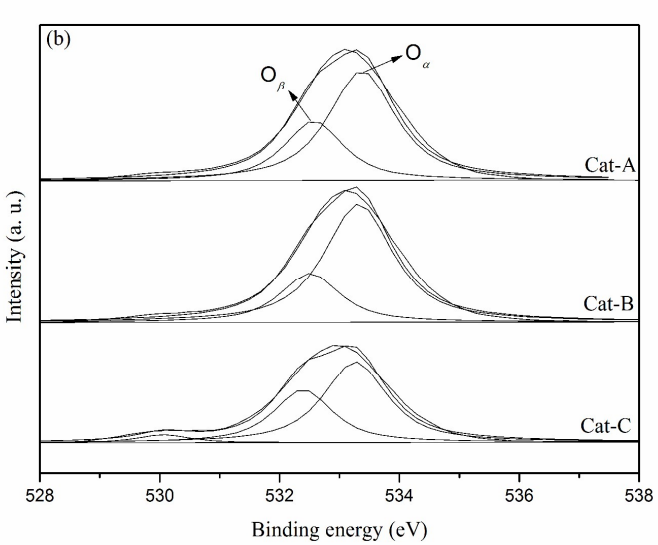

Fig. 5b O 1s XPS spectra of the catalysts.

Fig. 5b exhibited the O1s XPS spectra of the Cat-A, Cat-B and Cat-C catalysts. The O 1s peaks at 531.5-532.3 eV were assigned to the lattice oxygen (marked as O_β) [36, 37]. And the other peak at 532-533 eV could be attributed to the chemisorbed oxygen (marked as O_α) [38]. In order to reflect the variation of oxygen species, the percentage of the chemisorbed oxygen and lattice oxygen were measured by Gaussian curve fitting and the data were shown in Table 3. The $O_\alpha/(O_\alpha + O_\beta)$ ratio of Cat-A, Cat-B and Cat-C was 67.7%, 73.7% and 59.4%, respectively.

3.6 H_2-TPR analysis

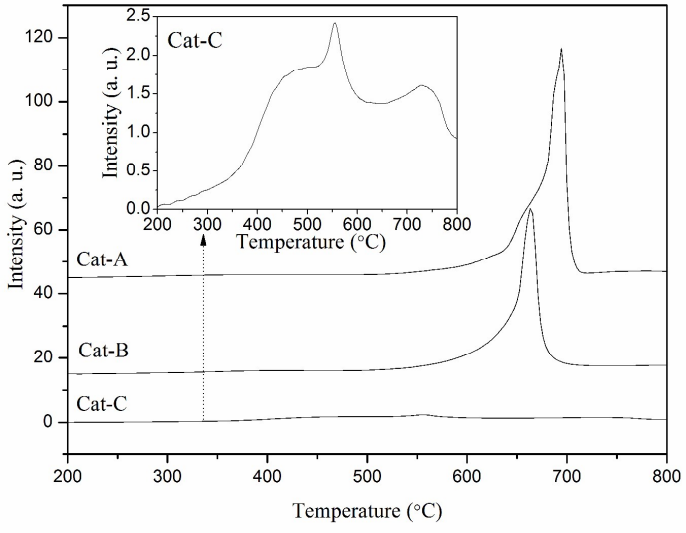

Fig. 6 H_2-TPR results of the catalysts.

The reducibility of Cat-A, Cat-C and Cat-B was characterized by H_2-TPR experiments and the results were exhibited in Fig. 6. The reduction peaks of the surface CeO_2 and the bulk CeO_2 over pure CeO_2 were located at 509 and 800 °C, respectively [39]. For the Cat-C catalyst, TPR curve consisted of two peaks: the low-temperature peak and the high-temperature peak, which was ascribed to the reduction of surface CeO_2 and bulk CeO_2, respectively. But the intensity reduction peaks of Cat-C were much weaker than those of Cat-A and Cat-B. The Cat-A catalyst with a shoulder peak at 660 ºC exhibited a sharp reduction peak at 694 °C, corresponding to the reduction of surface CeO_2 and sulfated species. It was obvious that the Cat-B catalyst showed merely one reduction peak at 665 ºC, which was attributed to the reduction of sulfated species. Compared with Cat-B and Cat-C, the reduction temperature of surface CeO_2 and sulfated species over Cat-A both shifted to higher temperatures, the reason of which might be that the strongest interaction between Ce, SO_4^{2-} and support existed. Besides, no reduction of sulfated species and CeO_2 were observed over Cat-B and Cat-C, respectively. Furthermore, the intensity reduction peak of sulfated species over Cat-A was stronger than that of Cat-B. The phenomena indicated that the redox properties of Cat-A, Cat-B and Cat-C were dramatically affected by the surface species and structure.

3.7 NH_3-TPD analysis

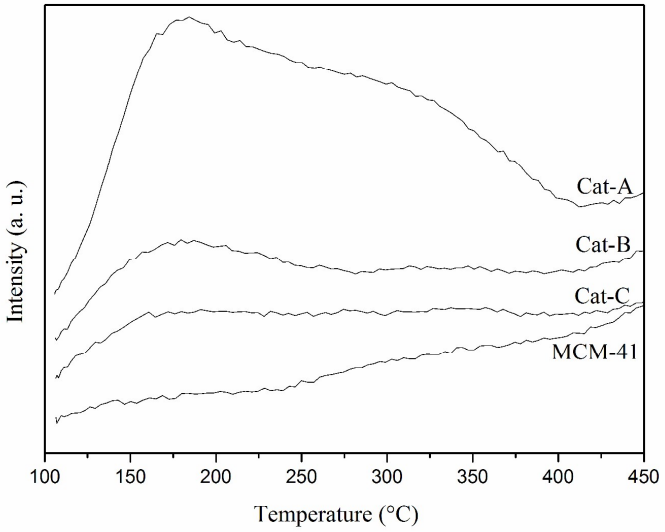

Fig. 7 NH_3-TPD results of the catalysts

NH_3-TPD analysis was performed in order to investigate the effect of surface acidity over Cat-A, Cat-B and Cat-C. As shown in Fig. 7, Cat-A showed two NH_3-desorption peaks: the first one centered at 175 °C, attributing to the weak acidity; and the other one located at 320 ºC, corresponding to the medium acidity [40]. Weaker peaks were observed at 100-250 °C on the Cat-B and Cat-C when compared with that of Cat-A, implying that Cat-A possessed more amount of weakly bound NH_3 sites. However, the intensity peaks of NH_3 desorption over Cat-A, Cat-B and Cat-C were remarkably higher than that of pure MCM-41, which meant that the surface acidity over the catalysts was greatly improved by the introduction of CeO_2 and SO_4^{2-} species into MCM-41. In addition, the NH_3-TPD results also revealed that the amount and distribution of surface acidity were affected significantly by the different structures and surface species over Cat-A, Cat-B and Cat-C.

3.8 The SCR activity of the catalysts

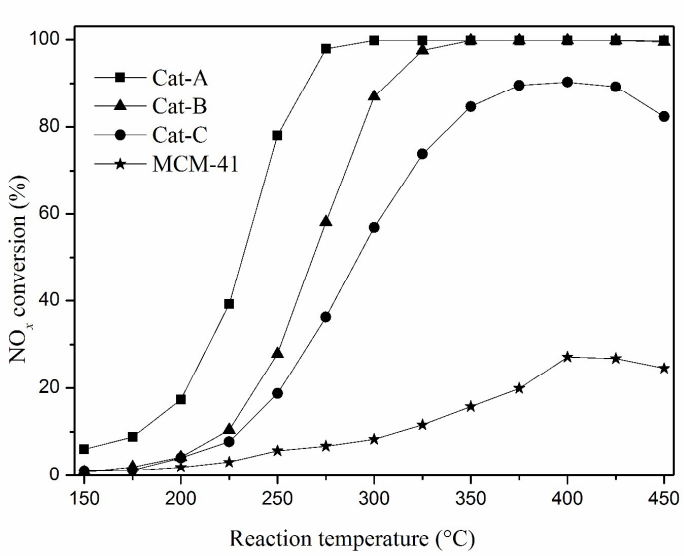

Fig. 8 NO_x conversion for the catalysts.

The catalytic activities of the Cat-A, Cat-B and Cat-C catalysts were shown in Fig. 8. Pure MCM-41 exhibited inferior catalytic activity and its maximum NO_x conversion was about 35% at 400 ºC. With the addition of $Ce(NO_3)_3 \cdot 6H_2O$ and SO_4^{2-} species into MCM-41, the SCR performance was dramatically enhanced. The Cat-C catalyst exhibited slight NH_3-SCR activity and 18.7% NO_x conversion was attained at 250 °C. With the increase of temperature, the Cat-C catalyst showed above 80% NO_x conversion at 337-450 °C. For the Cat-B catalyst, the SCR activity was dramatically promoted, its light-off temperature T50 (NO_x conversion was 50%) was about 268 °C

and over 80% NO_x conversion was in the temperature range of 294-450 °C. The T50 of Cat-A decreased to 230 °C and more than 80% NO_x conversion was 252-450 °C. It was obvious that the catalytic activity of Cat-A was evidently higher than Cat-B and Cat-C with the same components but different surface species and structures, which resulted in different SCR performance. Consequently, the catalytic activities of the catalysts were affected by the surface species and structure of Cat-A, Cat-B and Cat-C, and Cat-A showed the best catalytic activity.

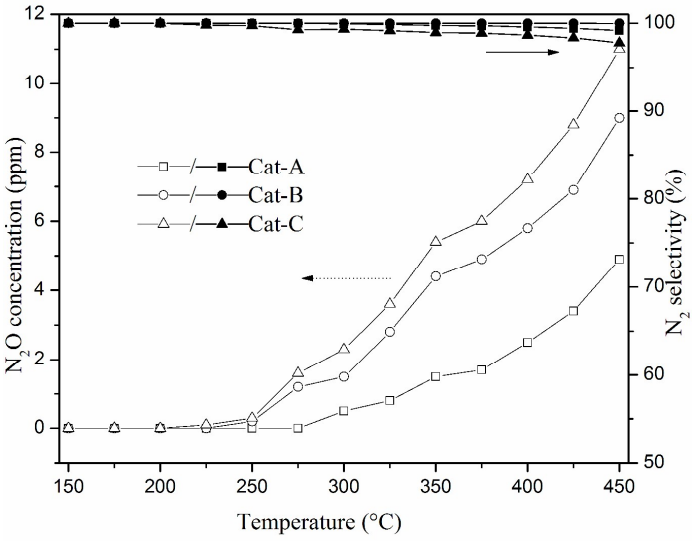

Fig.9 N_2O production and N_2 selectivity of the catalysts

The results of N_2O production and N_2 selectivity of Cat-A, Cat-B and Cat-C catalysts were exhibited in Fig. 9. The low N_2O production (below 12 ppm) was generated over the samples. Above 97% N_2 selectivity of Cat-A, Cat-B and Cat-C was attained at 150-450 ºC. The Cat-A, Cat-B and Cat-C catalysts showed the excellent N_2 selectivity in the temperature range of 150-450 ºC. Hence, the CeO_2 and SO_4^{2-} species doped into MCM-41 was a promising environmentally-friendly SCR catalyst.

3.9 NO oxidation

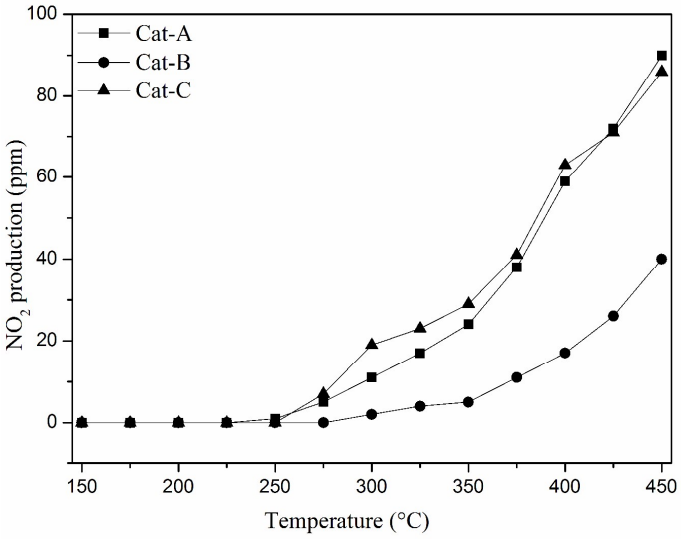

Fig. 10 NO oxidation activity over the Cat-A, Cat-B and Cat-C catalysts.

In order to investigate NO oxidation ability of the Cat-A, Cat-B and Cat-C catalysts, the properties of NO oxidation to NO_2 were exhibited in Fig. 10. It was obvious that NO_2 productions of Cat-A and Cat-C were remarkably higher than that of Cat-B at 150-450 ºC. These indicated that Cat-A and Cat-C showed the excellent oxidation ability. Roy et al. [41] reported that the evident difference of NH_3-SCR catalysts in NO oxidation ability and SCR performance could assigned to the role of NH_3 during the SCR process. Therefore, the surface acidity played an important role in NO oxidation activity. Combined with the SCR activity and NH_3-TPD results, Cat-C with the weakest surface acidity showed the least SCR performance. This indicated that the NO oxidation ability over Cat-A, Cat-B and Cat-C was not the only factor for determining the catalytic activity.

3.10 NH_3 oxidation

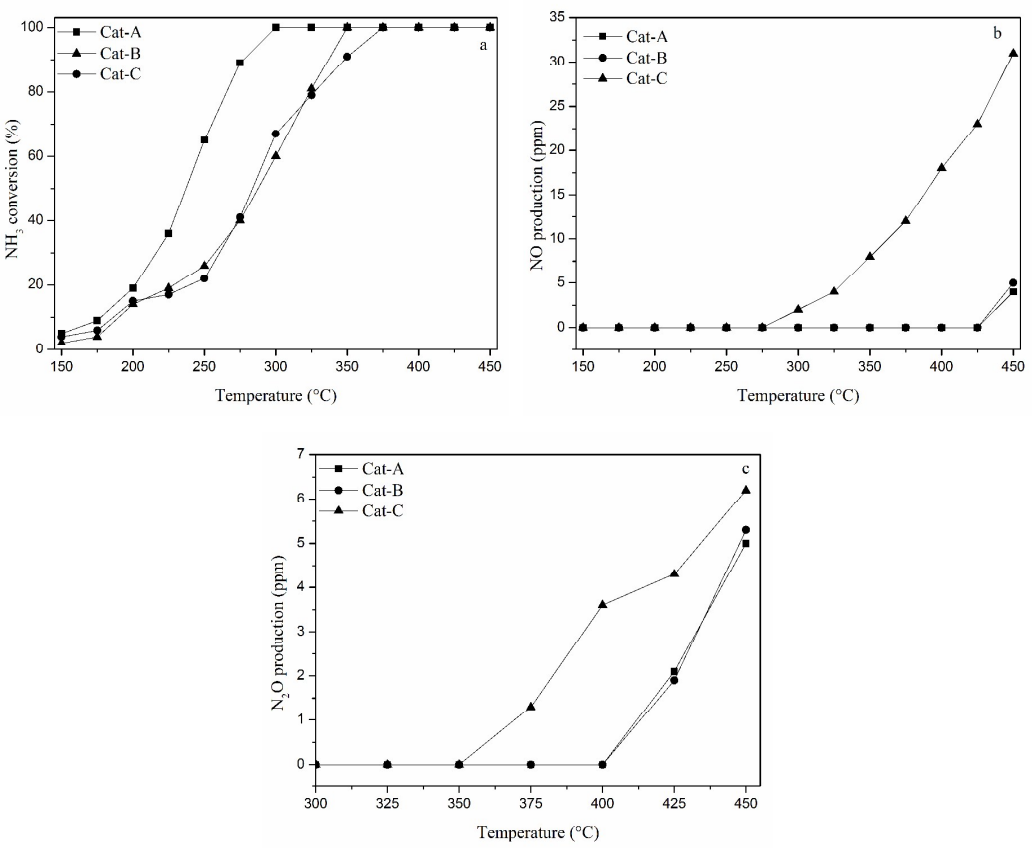

Fig. 11 NH_3 oxidation activity (a) and by-products over the catalysts: NO concentration (b); and N_2O concentration (c).

The NH_3 oxidation activity and by-products (N_2O, NO and NO_2) of the Cat-A, Cat-B and Cat-C catalysts were shown in Fig. 11. The NH_3 conversion of Cat-A was higher than those of Cat-B and Cat-C, especially for low temperature (below 300 ºC). And the NH_3 conversion decreased as follows: Cat-A > Cat-B ≈ Cat-C. The concentration of NO and N_2O over Cat-C was dramatically higher than that of Cat-A and Cat-B. The NO_2 production was not detected at 150-450 ºC and N_2O production was detected at higher temperatures (above 350) ºC over Cat-A, Cat-B and Cat-C. It was well known that the excellent redox property could result in the unwanted NH_3 unselective oxidation, causing the negative NO_x conversion at high temperatures. From the H_2-TPR results, Cat-C showed the lowest reduction temperature, which contributed to NH_3 unselective oxidation. Thereby, Cat-C possessed inferior catalytic activity at high temperatures. It was reported that the surface acidity played an important role in activating NH_3, which was the necessary steps in the NH_3-SCR reaction, resulting in enhancement of the catalytic activity and N_2 selectivity [42]. The formation of sulfated species over Cat-A and Cat-C could contribute to surface acidity,

remained a proper redox ability, and then weakened the NH_3 unselective catalytic oxidation, leading to the enhanced N_2 selectivity and SCR activity. Consequently, the surface acidity could contribute to the NH_3 conversion and catalytic activity. Combined with the NH_3-TPD and SCR performance results, Cat-A possessed the excellent NH_3 conversion and SCR activity in comparison with Cat-B and Cat-C, which might be ascribed to the abundance of weak and medium surface acidity.

Table 4 BET measurements for the A-Cat-A, A-Cat-B and A-Cat-C catalysts.

Samples	BET (m^2/g)	Total pore volume (cm^3/g)	Average pore diameter (nm)
A-MCM-41	921	0.9785	3.38
A-Cat-A	412	0.1468	5.83
A-Cat-B	100	0.1164	7.55
A-Cat-C	478	0.3703	3.57

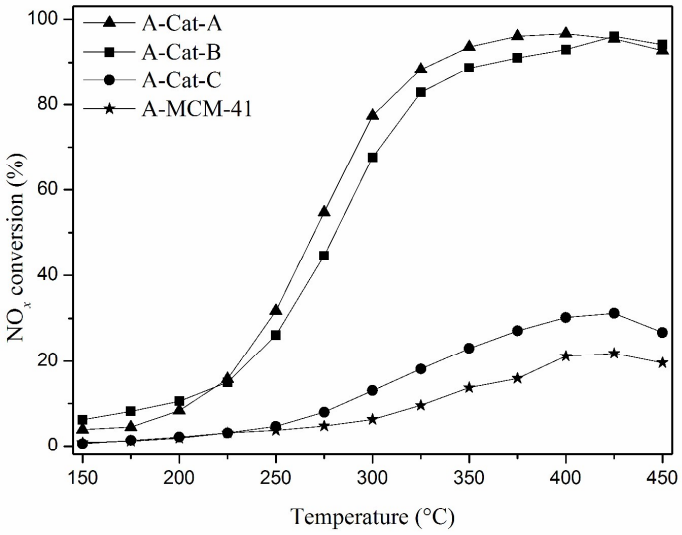

Fig. 12 NO_x conversion for the aged catalysts.

In order to elucidate the effect of surface species and structure on the SCR performance over the catalysts, pure MCM-41, Cat-A, Cat-B and Cat-C were calcinated at 650 ºC for 4 h and named as A-MCM-41, A-Cat-A, A-Cat-B and A-Cat-C, respectively. The BET surface areas, pore volumes and average pore diameters of the A-Cat-A, A-Cat-B and A-Cat-C catalysts, the results were shown in Table 4. The BET surface areas ranked in the sequence of A-Cat-C (478) > A-Cat-A (412) > A-Cat-B (100). From Fig. 12, A-Cat-A exhibited the best catalytic activity,

followed by A-Cat-B, and A-Cat-C showed the inferior performance. When the calcination temperature was 650 ºC, a portion of sulfated species would be decomposed from the TGA results; the structure would be destroyed under high temperature treatment, and then led to the decrease of catalytic activity in either event (the decomposition of sulfated species or the collapse of structure). Furthermore, pure A-MCM-41 possessed lager BET surface area (921 m^2/g) compared with that of the three aged samples, but it showed quite poor SCR activity. No obvious linear dependence between the catalytic activity and the BET surface areas was established. In addition, the catalytic activities of A-Cat-A, A-Cat-B and A-Cat-C were decreased when compared with those of the fresh samples. Thereby, it was reasonable that the decomposition of sulfated species could result in the deactivation over the samples. Consequently, the formation of sulfated species over MCM-41 modified by $Ce(NO_3)_3 \cdot 6H_2O$ and SO_4^{2-} contributed to the improvement of SCR activity.

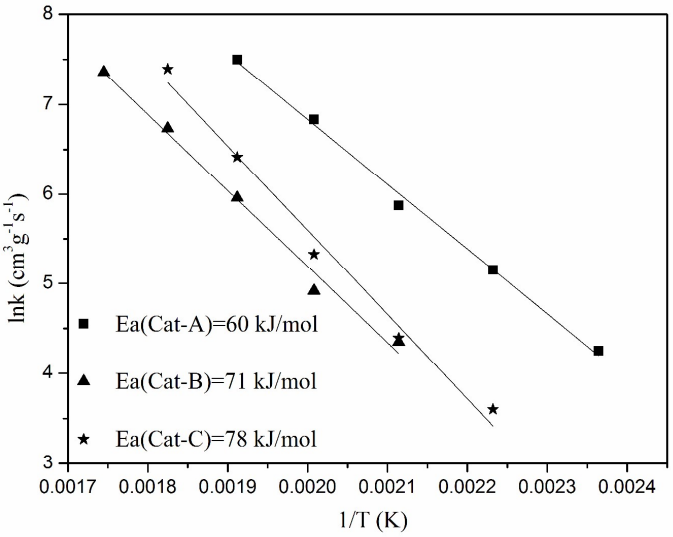

Fig. 13 Arrhenius plots for NO_x conversion over different catalysts.

To investigate the effect of the surface species and structure on catalytic activity over the Cat-A, Cat-B and Cat-C catalysts, the SCR performance was studied by the macro-kinetic approach and the results were shown in Fig. 13. Generally speaking, with respect to NO, the NH_3-SCR reaction was a first-order reaction [43, 44]. Therefore, the effective first-order rate constant was related to NO conversion by:

$$k = -\frac{V}{W} ln(1-x); \quad k = A\exp(-E_a / RT)$$

where k: reaction constant ($cm^3/g \cdot s$); V: the total gas flow rate (mL/s); W: the catalyst weight (g); x: the NO conversion (%); A: the pre-exponential factor; R: the

gas constant (8.3145 J/mol·K); T: the temperature (K); E_a: the apparent activation energy (kJ/mol). The measured activation energies of NO conversion over Cat-A, Cat-B and Cat-C were 60, 78 and 71 kJ/mol, respectively (Fig. 13). These differences originated from the different samples with the same components but different surface species and structure. The different surface species and structures over Cat-A, Cat-B and Cat-C should be further discussed because that the performance of the samples was significantly affected by the different structures, redox properties and surface species. Combined with the XRD and BET results, the particle sizes of CeO_2 over Cat-A was smaller than the other two samples. It was reported [45] that excellent dispersion of metal species on the support contributed to the catalytic activity of supported metal catalysts, which might be another reason that the Cat-A catalyst showed the superior SCR performance. However, the Cat-A catalyst possessed the least BET surface area for the fresh samples. The reason was that the small pores were blocked or filled by the formation of sulfate species, resulting in the disappearance of small pores and then a decrease in the specific surface area. Meanwhile, the Cat-A catalyst exhibited the best catalytic activity due to the formation of sulfated species. From the TGA results, the sulfated species were existed on the Cat-A and Cat-B catalysts, and the weight loss of Cat-A was more evident than that of Cat-B and Cat-C at 30-150 °C, indicating the occurrence of the largest number of hydroxyl over Cat-A, which contributed to the surface acidity, and then resulted in the excellent catalytic activity. Taking the SCR performance results into account, the catalytic activity ranked as follows: Cat-A > Cat-B > Cat-C. This phenomenon further confirmed that the SCR activity was dramatically improved by the formation of sulfated species. Considering the Raman, XPS and H_2-TPR results, the occurrence of the interaction between Ce, SO_4^{2-} and MCM-41 led to a difficulty in reducing the surface CeO_2 and sulfated species over the Cat-A catalyst. However, the sulfation could contribute to the formation of Ce^{3+} concentration and surface acidity. The higher $Ce^{3+}/(Ce^{3+} + Ce^{4+})$ ratio led to more oxygen vacancies, unsaturated chemical bonds and a charge imbalance, which was beneficial to the activation and transportation of active oxygen species, resulting in the improvement of SCR activity. The surface acidity could contribute to the adsorption of ammonia and then improve the catalytic activity. Hence, the sequence of catalytic activities over Cat-A, Cat-B and Cat-C was the same as that of $Ce^{3+}/(Ce^{3+} + Ce^{4+})$ ratio and amount of surface acidity. These also

confirmed that the formation of sulfated species on the surface of MCM-41 could contribute to the SCR activity. Meanwhile, the $O_\alpha/(O_\alpha + O_\beta)$ of Cat-A (67.7%) was lower than that of Cat-B (73.7%), which was due to the formation of sulfated species and then covered on the surface of Cat-A, leading to a decrease in surface oxygen species. Therefore, the catalytic activity of Cat-A, Cat-B and Cat-C was depended on the different surface species and structures.

3.11 The effect of H_2O and SO_2 on SCR activity

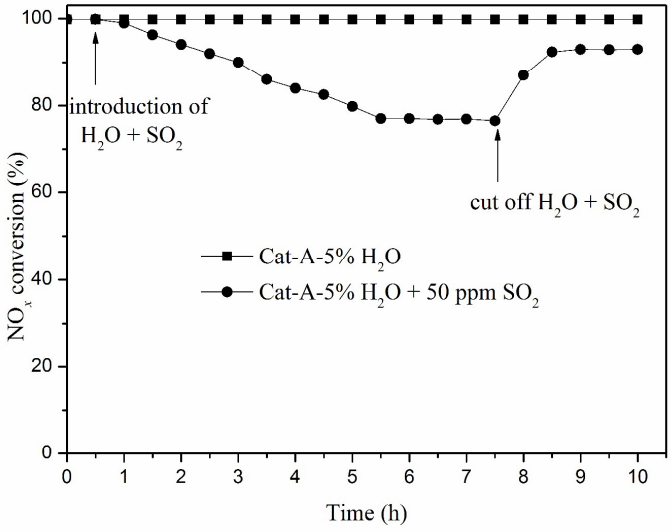

Fig. 14 The effect of H_2O and SO_2 on SCR activity over Cat-A

The emission of SO_2 and H_2O was unavoidable in exhaust gases from power plant. Therefore, the effect of SO_2 and H_2O on the SCR performance should not be ignored. Fig. 14 presented the effect of SO_2 and H_2O on the catalytic activity at 350 °C over the Cat-A, Cat-B and Cat-C catalysts. As shown in Fig. 14, Nearly 100% NO_x conversion of Cat-A was obtained in the presence of 5 vol.% H_2O, and no decrease in SCR activity was observed for 9.5 h. When 5 vol.% H_2O and 50 ppm SO_2 were added, the NO_x conversion of Cat-A was decreased. However, almost 80% NO_x conversion still was attained during the measured period. Although the NO_x conversion could not recover to its original value after 5 vol.% H_2O and 50 ppm SO_2 were cut off. However, the Cat-A catalyst still exhibited the superior SCR performance and 97% NO_x conversion was obtained. Thereby, Cat-A possessed the excellent SO_2+H_2O durability.

4. Conclusions

The present work investigated the effect of surface species and structure on the SCR activity of CeO_2 and SO_4^{2-} doped MCM-41 support. The results revealed that

Cat-A showed the best SCR performance and above 80% NO_x conversion was obtained in the temperature range of 294-450 °C. The XRD results suggested that Cat-A possessed the smallest CeO_2 particle sizes. The BET results suggested that the specific surface area was not the only factors affecting the catalytic activity. The Raman and H_2-TPR results implied that the interaction between Ce, SO_4^{2-} and MCM-41 existed and the sulfated species formed over Cat-A and Cat-B, which could affect the redox ability. The TGA results indicated that the sulfated species were generated over Cat-A and Cat-B. The XPS and NH_3-TPD results proved that Cat-A possessed higher surface $Ce^{3+}/(Ce^{3+} + Ce^{4+})$ ratio and the more amount of surface acid sites. The apparent activation energy of Cat-A, Cat-B and Cat-C was 60, 71 and 78 kJ/mol, respectively. These above factors depended on the structure and surface species over CeO_2 and SO_4^{2-} doped MCM-41, which could in turn affect the catalytic activity.

5. Acknowledgements

This work is supported by the National Natural Science Foundation of China (No.21307047) and Academic Newcomer Award of Yunnan Province.

6. References

[1] C. H. He, Y. H. Wang, Y. S. Cheng, K. L. Christine, R. T. Yang, Activity, stability and hydrocarbon deactivation of Fe/Beta catalyst for SCR of NO with ammonia, *Appl. Catal. A: Gen.,* 2009, 368, 121-126.

[2] B. Guan, R. Zhan, H. Lin, Z. Huang, Review of state of the art technologies of selective catalytic reduction of NO_x from diesel engine exhaust, *Appl. Thermal Eng.,* 2014, 66, 395-414.

[3] T. V. W. Janssens, H. Falsig, L. F. Lundegaard, P. N. R. Vennestrøm, S. B. Rasmussen, P. G. Moses, F. Giordanino, E. Borfecchia, K. A. Lomachenko, C. Lamberti, S. Bordiga, A. Godiksen, S. Mossin, P. Beato, A Consistent Reaction Scheme for the Selective Catalytic Reduction of Nitrogen Oxides with Ammonia. *ACS Catal.,* 2015, 5, 2832-2845

[4] I. Lezcano-Gonzalez, U. Deka, H. E. van der Bij, P. Paalanen, B. Arstad, B. M. Weckhuysen, A. M. Beale, Chemical deactivation of Cu-SSZ-13 ammonia selective catalytic reduction (NH_3-SCR) systems, *Appl. Catal. B-Environ.,* 2014, 154-155,

339-349.

[5] Q. L. Zhang, C. T. Qiu, H. D. Xu, T. Lin, M. C. Gong, Y. Q. Chen, Novel promoting effects of tungsten on the selective catalytic reduction of NO by NH_3 over MnO_x-CeO_2 monolith catalyst, *Catal. Commun.,* 2011, 16, 20-24.

[6] J. Qiu, K. Zhuang, M. Lu, B. L. Xu, Y. N. Fan, The selective catalytic reduction activity of Cu/MCM-41 catalysts prepared by using the Cu^{2+}-MCM-41 mesoporous materials with copper ions in the framework as precursors, *Catal. Commun.,* 2013, 31, 21-24.

[7] V. Parvulescu, B. L. Su. Iron, cobalt or nickel substituted MCM-41 molecular sieves for oxidation of hydrocarbons, *Catal. Today,* 2001, 69, 315-322.

[8] B. Lindlar, A. Kogelbauer, R. Prins, Chemical, structural, and catalytic characteristics of Al-MCM-41 prepared by pH-controlled synthesis, *Micropor. Mesopor. Mater.,* 2000, 38, 167-176.

[9] A. Hagen, K. Schueler, F. Roessner, The performance of Ti-MCM-41 in aqueous media and after mechanical treatment studied by in situ XANES, UV/Vis and test reactions, *Micropor. Mesopor. Mater.,* 2002, 51, 23-33.

[10] A. B. Sorokin, A. Tuel, Metallophthalocyanine functionalized silicas: catalysts for the selective oxidation of aromatic compounds, *Catal. Today,* 2000, 57, 45-59.

[11] C. C. Liu, H. S. Teng, Cu/MCM-41 for selective catalytic NO reduction with NH_3—comparison of different Cu-loading methods, *Appl. Catal. B-Environ.,* 2005, 58, 69-77.

[12] Y. Wan, J. X. Ma, Z. Wang, W. Zhou, S. Kaliaguine, On the mechanism of selective catalytic reduction of NO by propylene over Cu-Al-MCM-41, *Appl. Catal. B-Environ.,* 2005, 59, 235-242.

[13] J. Qiu , K. Zhuang, M. Lu, B. L. Xu, Y. N. Fan, The selective catalytic reduction activity of Cu/MCM-41 catalysts prepared by using the Cu^{2+}-MCM-41 mesoporous aterials with copper ions in the framework as precursors, *Catal. Commun.,* 2013, 31, 21-24.

[14] M. Ziolek, I. Sobczak, I. Nowak, P. Decyk, A. Lewandowska, J. Kujawa, Nb-containing mesoporous molecular sieves—a possible application in the catalytic processes, *Micropor. Mesopor. Mater.,* 2000, 35-36, 195-207.

[15] J. R. Sohn, S. H. Lee, J. S. Lim, New solid superacid catalyst prepared by doping ZrO_2 with Ce and modifying with sulfate and its catalytic activity for acid catalysis,

Catal. Today, 2006, 116, 143-150.

[16] S. Gao, X. B. Chen, H. Q. Wang, J. S. Mo, Z. B. Wu, Y. Liu, X. L. Weng, Ceria supported on sulfated zirconia as a superacid catalyst for selective catalytic reduction of NO with NH_3, *J. Colloid Interf. Sci.,* 2013, 394, 515-521.

[17] D. Pietrogiacomi, A. Magliano, P. Ciambelli, D. Sannino, M. C. Campa, V. Indovina, The effect of sulphation on the catalytic activity of CoO_x/ZrO_2 for NO reduction with NH_3 in the presence of O_2, *Appl. Catal. B-Environ.,* 2009, 89, 33-40.

[18] X. S. Du, X. M. Wang, Y. R. Chen, X. Gao, L. Zhang, Supported metal sulfates on Ce-TiO_x as catalysts for NH_3-SCR of NO: High resistances to SO_2 and potassium, *J. Ind. Eng. Chem.,* 2016, 36, 271-278.

[19] M. Yonemitsu, Y. Tanaka, M. Iwamoto, Metal ion-planted MCM-41 2. Catalytic epoxidation of stilbene and its derivatives with tert-butyl hydroperoxide on Mn-MCM-41, *J. Catal.,* 1998, 178, 207-213.

[20] Y. Wang, Y. Ohishi, T. Shishido, Q. Zhang, W. Yang, Q. Guo, H. Wan, K. Takehira, Characterizations and catalytic properties of Cr-MCM-41 prepared by direct hydrothermal synthesis and template-ion exchange, *J. Catal.,* 2003, 220, 347-357.

[21] F. Zhang, S. W. Chan, J. E. Spanier, E. Apak, Q. Jin, Cerium oxide nanoparticles: size-selective formation and structure analysis, *Appl. Phys. Lett.,* 2002. 80, 127-129.

[22] B. Guan, H. Lin, L. Zhu, B. Tian, Z. Huang, Effect of ignition temperature for combustion synthesis on the selective catalytic reduction of NO_x with NH_3 over $Ti_{0.9}Ce_{0.05}V_{0.05}O_{2-\delta}$ nanocomposites catalysts prepared by solution combustion route, *Chem. Eng. J.,* 2012, 181-182, 307-322.

[23] X. N. Wei, X. Shi, Mesoporous zirconium phenylphosphonates for selective enrichment of phosphopeptides, *J. Phys. Chem. C,* 2014, 118, 4213-4221.

[24] H. Wan, J.N. Li, W.G. Yu, Z.Y. Liu, Q.Q. Zhang, W.B. Zhang, H.F. Zou, Fabrication of a novel magnetic yolk-shell Fe_3O_4@mTiO_2@mSiO_2 nanocomposite for selective enrichment of endogenous phosphopeptides from a complex sample, *RSC Adv.,* 2014, 4, 45804-45808.

[25] M. Jaroniec, M. Kruk, H. Shin, R. Ryoo, Y. Sakamoto, O. Terasaki, Comprehensive characterization of highly ordered MCM-41 silicas using nitrogen adsorption, thermogravimetry, X-ray diffraction and transmission electron microscopy, *Microporous Mesoporous Mater.* 2001, 48, 127-134.

[26] M. Thommes, B. Smarsly, M. Groenewolt, P. Ravikovitch, A. Neimark, Adsorption hysteresis of nitrogen and argon in pore networks and characterization of novel micro- and mesoporous silicas, *Langmuir,* 2006, 22, 756-764.

[27] J. P. Wang, Z. Yan, L. L. Liu, Y. Y. Zhang, Z. T. Zhang, X. D. Wang, Low-temperature SCR of NO with NH_3 over activated semi-coke composite-supported rare earth oxides, *Appl. Surf. Sci.,* 2014, 309, 1-10.

[28] L. Ilieva, G. Pantaleo, I. Ivanov, A.M. Venezia, D. Andreeva, Gold catalysts supported on CeO_2 and CeO_2-Al_2O_3 for NOx reduction by CO, *Appl. Catal. B-Environ.,* 2006, 65, 101-109.

[29] X. Q. Wang, J. A. Rodriguez, J. C. Hanson, D. Gamarra, A. Martínez-Arias, M. Fernández-García, Unusual physical and chemical properties of Cu in $Ce_{1-x}Cu_xO_2$ Oxides, *J. Phys. Chem. B,* 2005, 109, 19595-19603.

[30] X. Q. Wang, J. A. Rodriguez, J. C. Hanson, D. Gamarra, A. Martínez-Arias, M. Fernández-García, In situ studies of the active sites for the water gas shift reaction over Cu-CeO_2 catalysts: Complex interaction between metallic copper and oxygen vacancies of ceria, *J. Phys. Chem. B,* 2006, 110, 428-434.

[31] D. W. Kwon, K. B. Nam, S. C. Hong, The role of ceria on the activity and SO_2 resistance of catalysts for the selective catalytic reduction of NO_x by NH_3, *Appl. Catal. B-Environ.,* 2015, 166-167, 37-44.

[32] X. Gao, Y. Jiang, Y. Zhong, Z. Y. Luo, K. F. Cen, The activity and characterization of CeO_2-TiO_2 catalysts prepared by the sol-gel method for selective catalytic reduction of NO with NH_3, *J. Hazard. Mater.,* 2010, 174, 734-739.

[33] S. Ricote, G. Jacobs, M. Milling, Y. Ji, P. M. Patterson, B. H. Davis, Low temperature water-gas shift: Characterization and testing of binary mixed oxides of ceria and zirconia promoted with Pt, *Appl. Catal. A: Gen.,* 2006, 303, 35-47.

[34] C. R. Vera, J. C. Yori, J. M. Parera, Redox properties and catalytic activity of SO_4^{2-}-ZrO_2 catalysts for n-butane isomerization: Role of transition metal cation promoters, *Appl. Catal. A: Gen.,* 1998, 167, 75-84.

[35] F. Dury, E. Gaigneaux, The deoxygenation of benzoic acid as a probe reaction to determine the impact of superficial oxygen vacancies (isolated or twin) on the oxidation performances of Mo-based oxide catalysts, *Catal. Today,* 2006, 117, 46-52.

[36] B. J. Dou, G. Lv, C. Wang, Q. L. Hao, K. S. Hui, Cerium doped copper/ZSM-5 catalysts used for the selective catalytic reduction of nitrogen oxide with ammonia. *Chem. Eng. J.,* 2015, 270, 549-556.

[37] Y. J. Kim, H. J. Kwon, I. Heo, I. Nam, B. K. Cho, J. W. Choung, M. Cha, G. K. Yeo, Mn-Fe/ZSM5 as a low-temperature SCR catalyst to remove NO_x from diesel engine exhaust, *Appl. Catal. B-Environ.,* 2012, 126, 9-21.

[38] H. Praliaud, S. Mikhailenko, Z. Chajar, M. Primet, Surface and bulk properties of Cu-ZSM-5 and Cu/A_2O_3 solids during redox treatments. Correlation with the selective reduction of nitric oxide by hydrocarbons, *Appl. Catal. B-Environ.,* 1998, 16, 359-374.

[39] S. Damyanova, C. A. Perez, M. Schmal, J. M. C. Bueno, Characterization of ceria-coated alumina carrier, Appl. Catal. A: Gen., 2002, 234, 271-282.

[40] Y. S. Shen, Y. F. Ma, S. M. Zhu, Promotional effect of zirconium additives on $Ti_{0.8}Ce_{0.2}O_2$ for selective catalytic reduction of NO. *Catal. Sci. Technol.*, 2012, 2: 589-599.

[41] S. Roy, B. Viswanath, M. S. Hegde, G. Madras, Low-temperature selective catalytic reduction of NO with NH_3 over $Ti_{0.9}M_{0.1}O_{2-\delta}$ (M= Cr, Mn, Fe, Co, Cu), *J. Phys. Chem. C,* 2008, 112*,* 6002-6012

[42] W. Zhao, Q. Zhong, Y. X. Pan, R. Zhang, Systematic effects of S-doping on the activity of V_2O_5/TiO_2 catalyst for low-temperature NH_3-SCR. *Chem. Eng. J.*, 2013, 228: 815-823.

[43] G. S. Qi, R. T. Yang, Performance and kinetics study for low temperature SCR of NO with NH_3 over MnO_x-CeO_2 catalyst, *J. Catal.,* 2003, 217, 434-441.

[44] G. S. Qi, R. T. Yang, R. Chang, MnO_x-CeO_2 mixed oxides prepared by co-Precipitation for selective catalytic reduction of NO with NH_3 at low temperatures, *Appl. Catal. B-Environ.,* 2004, 51, 93-106.

[45] T. Zhang, J. Liu, D. X. Wang, Z. Zhao, Y. C. Wei, K. Cheng, G. Y. Jiang, A. J. Duan, Selective catalytic reduction of NO with NH_3 over HZSM-5-supported Fe-Cu nanocomposite catalysts: the Fe-Cu bimetallic effect, *Appl. Catal. B-Environ.,* 2014, 148-149, 520-531.

Effect of surface species and structure on the performance of CeO_2 and SO_4^{2-} doped MCM-41 catalyst toward NH_3-SCR

Zhongxian Song [a], Xiang Wu [b], Qiulin Zhang [a*], Ping Ning [a**], Jie Fan [a], Xin Liu [a], Qixian Liu [a], Zhenzhen Huang [c]

([a]Faculty of Environmental Science and Engineering, Kunming University of Science and Technology. Kunming, 650500, P.R. China;[b]Yunnan TianAn Chemical Co., Ltd., Anning, 650309, P.R. China; [c]College of Environmental Science and Engineering, Hunan University, Changsha 410082, P.R. China)

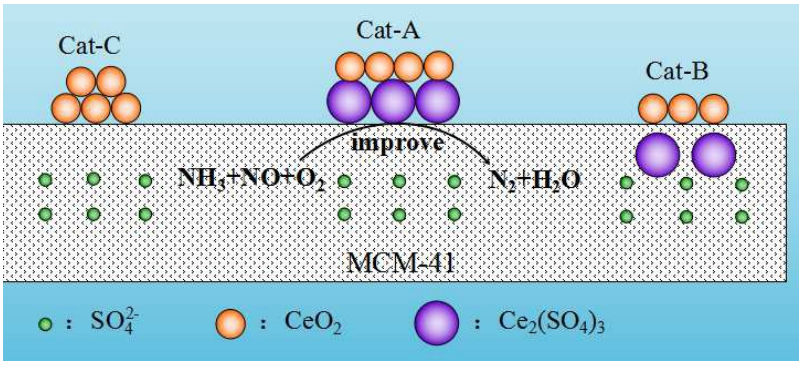

The different structure and surface species on the SCR activity of CeO_2 and SO_4^{2-} doped MCM-41 catalysts toward NO reduction by NH_3 were investigated. The sulfated species generated over Cat-A ($Ce(NO_3)_3 \cdot 6H_2O$ and H_2SO_4 simultaneously doped on MCM-41) and Cat-B ($Ce(NO_3)_3 \cdot 6H_2O$ firstly immerged to MCM-41 and followed by impregnation of H_2SO_4) except for Cat-C (H_2SO_4 firstly doped onto MCM-41 and followed by $Ce(NO_3)_3 \cdot 6H_2O$). The formation of sulfated species contributed to the surface acidity and then resulted in an enhancement of SCR activity.